Nonconvex Multiview Subspace Clustering Framework with Efficient Method Designs and Theoretical Analysis

Zhi Wang, **Zhuo Liu**, **Dong Hu** and **Tao Jia***
College of Computer and Information Science, Southwest University, Chongqing, China
chiw@swu.edu.cn, zhuoliu.swu@gmail.com, donghu@email.swu.edu.cn, tjia@swu.edu.cn

Abstract

Multi-view subspace clustering (MvSC) is one of the most effective methods for understanding and processing high-dimensional data. However, existing MvSC methods still have two shortcomings: (1) they adopt the nuclear norm as the low-rank constraint, which makes it impossible to fully exploit the mutually complementary subspace information, and (2) they do not handle disjoint and confounding points carefully, which may degrade the purity and distinctiveness of cross-view fusion. To address these issues, in this paper we propose a novel MvSC model with nonconvex ℓ_q regularization. Specially, our proposed model can not only effectively capture the intrinsic global low-rank structure, but also accurately cluster disjoint and confounding data samples into corresponding subspaces. Then, an efficient algorithm is developed with convergence guarantee. Furthermore, we prove that the sequence generated by our proposed algorithm converges to the desirable Karush-Kuhn-Tucker (KKT) critical point. Extensive experiments on various datasets verify the superiority of our proposed model. MATLAB code is available at https://github.com/wangzhi-swu/NLRSC-MvSC.

1 Introduction

In many real-world applications, one needs to consider how to effectively and efficiently process high-dimensional data, which is a key issue in machine learning [Slepčev and Thorpe, 2019; Cai *et al.*, 2011; Tang *et al.*, 2023], computer vision [Ho *et al.*, 2003; Yang *et al.*, 2008; Vidal *et al.*, 2008], and pattern recognition [Basri and Jacobs, 2003; Ma *et al.*, 2008]. However, such problems are extremely challenging because of the “curse of dimensionality” [Muja and Lowe, 2014]. Fortunately, some researchers have pointed out that high-dimensional data are drawn from low-dimensional subspaces. Therefore, how to efficiently recover the low-dimensional structures in datasets becomes a crucial step.

To address this issue, *subspace clustering* (SC) has been proposed and extensively studied, and has become the most important and fundamental tool for high-dimensional data analysis [Vidal, 2011; Liu *et al.*, 2010]. Such technique aims to separate data samples into their exclusive groups, where each group corresponds to a subspace with highly similar characteristics. The most prevalent methods of self-representation based subspace clustering are *sparse subspace clustering* (SSC) [Elhamifar and Vidal, 2013], *low-rank representation* (LRR) [Liu *et al.*, 2012], and some of their variants [Qu *et al.*, 2022; Liu *et al.*, 2023c]. Specifically, SSC has the ability to seek the sparsest representation coefficients corresponding to the data from the same subspace. On the other hand, LRR is to seek a low-rank subspace representation. Despite their success, these approaches only focus on single-view features.

In practical scenarios, however, data are often collected from different sources and can be represented by various types of features [Fang *et al.*, 2023]. For example, a color image consists of colors, textures, and shapes, a video is a combination of visual frames and audio tracks, and a web page may contain text, images and their corresponding link. The features of different views usually have their own inherent attributes, which make it possible to provide consistent and complementary information to each other. Therefore, integrating these different heterogeneous and complementary features into clustering methods can significantly improve their performance.

To exploit complementary and consistent information from different views, many *Multi-view* SC (MvSC) methods have been proposed [Gao *et al.*, 2015; Zhang *et al.*, 2017; Li *et al.*, 2019a; Chen *et al.*, 2022]. Different from single-view subspace clustering methods, MvSC uses multiple features to accomplish the multi-view data clustering tasks. Therefore, the MvSC methods have superiority compared with single-view subspace clustering methods. Although these methods have achieved remarkable results in MvSC tasks, they still suffer from the following shortcomings. First, they adopt the convex nuclear norm as the low-rank constraint, which ignores significant differences between different singular values [Wang *et al.*, 2021; Wang *et al.*, 2022; Shan *et al.*, 2023]. As a result, they cannot accurately capture low rankness, resulting in inferior performance. Second, the union of underlying n subspaces $\{S_i\}_{i=1}^{n}$ is commonly disjoint [Tang *et al.*, 2014]. As shown in Figure 1, for the data points that nearby distributed at local intersections, it is

*Corresponding author

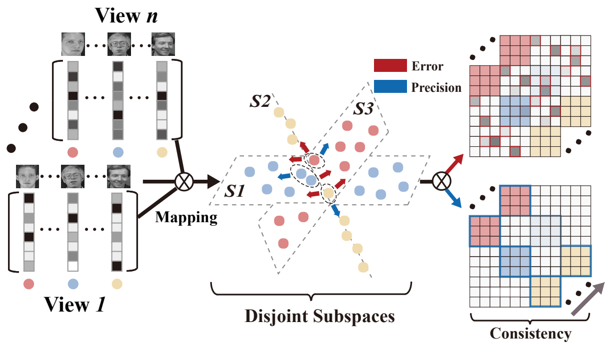

Figure 1: A toy example of disjoint subspaces, and the coefficient representations resulting from biased and exact clustering.

hard to identify the subspaces they really belong to. Unfortunately, these confounding points have still not been carefully handled, which may degrade the purity and distinctiveness of cross-view fusion.

To overcome above drawbacks, in this paper we propose a new MvSC model namely **N**onconvex **L**ow-**R**ank and **S**tructure-**C**onstrained MvSC (NLRSC-MvSC). Comparing with the aforementioned models, NLRSC-MvSC has two prominent advantages. First, by using the ℓ_q norm [Marjanovic and Solo, 2012] in our model, the intrinsic low-rank structure in multi-view data can be efficiently captured [Wang *et al.*, 2019; Wang *et al.*, 2020]. Thus, the mutually complementary subspace information embedding in each view can be fully exploited, so as to provide a more comprehensive and in-depth description with regard to the underlying subspaces. Second, with the aim of clustering the disjoint and confounding data samples into corresponding subspaces, a shared cross-view structure restriction is naturally imposed on each coefficient matrix. To be concrete, the correlation between inter-cluster samples can be significantly reduced with a soft penalty strategy, whereas the informative intra-cluster coefficients are sufficiently preserved. As a result, by fusing the view-specific compact representations, a more discriminative consensus fusion is yield, which can offer a better characterization of true subspace structure. In summary, the main highlights of this paper are as follows.

- We propose a novel MvSC model that simultaneously imposes low-rank and structural constraints on view-specific representations by leveraging the nonconvex ℓ_q norm and soft penalty strategy. It can comprehensively explore the complementary and consistent connections among multiple coefficient matrices, thereby further facilitating the effectual cross-view fusion.
- We establish an efficient algorithm to solve the corresponding optimization problem. Furthermore, rigorous mathematical proof shows that the sequence generated by our proposed algorithm converges to a KKT point.
- Extensive experiments on various multi-view datasets validate the effectiveness and superiority of our proposed model over several state-of-the-art multi-view clustering models.

2 Related Work

2.1 Multi-view Subspace Clustering

As a fundamental tool for processing multi-view data, MvSC has become an active topic in machine learning and computer vision in recent years. Generally speaking, most existing MvSC methods have three steps, including i) learn the coefficient matrices of the data samples via "self-expressiveness"; ii) construct the affinity graph by fusing the learned coefficient representations; iii) apply the spectral clustering method [Ng *et al.*, 2001] on affinity graph to get the final clustering result. How to accurately learn a coefficient matrix is crucial for these methods. To this end, the LRR strategy is commonly used to recover the underlying subspaces, which can fully capture the global structure of the data. However, the resultant optimization problem is NP-hard due to the discreteness of the rank function. To alleviate this problem, a common approach is to use nuclear norm as its convex relaxation. In real world, the multi-view data may contain errors (e.g., noise and outliers). Thus, the $\ell_{2,1}$ norm can be used to reduce their interference. Along this line of research, a large number of MvSC models have been proposed [Zhang *et al.*, 2017; Luo *et al.*, 2018; Chen *et al.*, 2022]. In [Zhang *et al.*, 2017], Zhang et al. proposed a latent MvSC (LMvSC) model to explore the complementarity of multiple views. In [Chen *et al.*, 2022], Chen et al. proposed a multi-view LRR (MvLRR) model by using symmetric LRR fusion, which can more comprehensively explore the underlying low-rank subspace. In [Luo *et al.*, 2018], Luo et al. proposed a model that can learn consistent and specific representations simultaneously. Although these methods have achieved satisfactory results in MvSC tasks, there are still some shortcomings. On the one hand, the nuclear norm as the low-rank constraint may result in a severe loss of multi-view information. On the other hand, these methods enforce the elements across representations to be consistent, which neglects the difference in value magnitudes between and within views.

2.2 Nonconvex $\ell_q (0 < q < 1)$ Regularization

In the region of compressed sensing [Chartrand, 2007; Chartrand and Yin, 2008], the nonconvex regularization methods related to the ℓ_q norm [Marjanovic and Solo, 2012] have received extensive attention, and a large number of theoretical results and algorithms have been proposed to solve the corresponding optimization problems. Comparing with its convex counterparts, using the ℓ_q norm can obtain more sparse solution and requires fewer measurements. In general, the minimization problem associated with ℓ_q norm can be solved by the following non-trivial optimization problem

$$\min_{x \geq 0} \left\{ f(x) = \lambda x^q + \frac{1}{2}(x-y)^2 \right\}, \tag{1}$$

where $\lambda > 0$ is a parameter. However, it is in general difficult to provide a thorough theoretical understanding for finding a global solution. Besides, how to choose a proper q to yield the best result is also an open issue. Fortunately, recent researches [Xu *et al.*, 2012; Cao *et al.*, 2013] have shown that the efficiency of $\ell_{1/2}$ and $\ell_{2/3}$ regularizations is very high, and their corresponding closed-form thresholding formulas can be easily obtained.

Lemma 1 ([Xu *et al.*, 2012]). *For any $\lambda > 0$, the optimal solution to*

$$\min_{x\geq 0} \lambda x^{\frac{1}{2}} + \frac{1}{2}(x-y)^2, \tag{2}$$

is given by

$$h_{\lambda,\frac{1}{2}}(x) = \begin{cases} \frac{2}{3}x(1+\cos(\frac{2\pi}{3} - \frac{2\psi_\lambda(x)}{3})), x > \gamma \\ 0, \quad \textit{otherwise}, \end{cases} \tag{3}$$

where $\psi_\lambda(x) = \arccos((\lambda/4)(x/3)^{-3/2})$ *and* $\gamma = 3\sqrt[3]{2}/4(2\lambda)^{2/3}$.

Lemma 2 ([Cao *et al.*, 2013]). *For any $\lambda > 0$, the optimal solution to*

$$\min_{x\geq 0} \lambda x^{\frac{2}{3}} + \frac{1}{2}(x-y)^2, \tag{4}$$

is given by

$$h_{\lambda,\frac{2}{3}}(x) = \begin{cases} \left(\frac{\varphi_\lambda(x)+\Phi_\lambda(x)}{2}\right)^3, x > \gamma \\ 0, \quad \textit{otherwise,} \end{cases} \tag{5}$$

where $\Phi_\lambda(x) = (2x/\varphi_\lambda(x) - \varphi_\lambda(x)^2)^{1/2}$ *with* $\varphi_\lambda(x) = (2/\sqrt{3})(2\lambda)^{1/4}(\cosh(\text{arccosh}(27x^2(2\lambda)^{-3/2}/16)/3))^{1/2}$ *and* $\gamma = 2/3(3(2\lambda)^3)^{1/4}$.

Accordingly, to improve the efficiency of our proposed method without sacrificing performance, we only consider the nonconvex ℓ_q regularization with $q \in \{1/2, 2/3\}$.

3 Methodology

This section firstly formulates the proposed NLRSC-MvSC model by utilizing the cross-view and underlying structure information comprehensively. Then, an effective algorithm with convergence guarantee is devised to address the resultant optimization problem.

3.1 Problem Definition

Given multi-view data $X = \{\mathbf{X}_1, \mathbf{X}_2, \ldots, \mathbf{X}_V\}$, where each $\mathbf{X}_v \in \mathbb{R}^{d_v \times n}$ denotes the v-th feature matrix. The purpose of MvSC is to divide the given samples into k groups. To improve the performance of MvSC method, the two general prior principles, i.e., *Complementarity* and *Consistency*, should be fully considered.

Complementarity. In most practices, one data object can be described by different subspace information from multiple views, which are commonly complementary with each other. Therefore, it is of prime importance to maximize the diversity of joint representations so as to pursue a comprehensive information fusion. To this end, by leveraging the superior ℓ_q norm and subspace self-expressiveness property, a nonconvex low-rank MvSC model is proposed

$$\begin{aligned} &\min_{\mathbf{C}_v,\mathbf{E}_v} \sum_{v=1}^{V} \|\mathbf{C}_v\|_q^q + \beta \sum_{v=1}^{V} \|\mathbf{E}_v\|_{2,q}, \\ &\quad \text{s.t. } \mathbf{X}_v = \mathbf{X}_v\mathbf{C}_v + \mathbf{E}_v, \forall v \in \{1, 2, \ldots, V\}, \end{aligned} \tag{6}$$

where $\mathbf{C}_v$ denotes the v-th view's learned subspace representation, $\mathbf{E}_v$ denotes the error matrix for characterizing the noise and outliers, $\beta > 0$ denotes a balance parameter, and the $\ell_{2,q}$ norm is a sparser error characteristic than $\ell_{2,1}$ due to the embedding of ℓ_q penalty.

Consistency. It is well known that all the view representations exhibit a common block diagonal structure with different value magnitudes. Instead of forcing each pair of them tend to be similar, we advocate to enhance the consistent block diagonal property across representation matrices, while retaining the diversity within them. Thus, a shared structural constraint on each subspace representation is introduced into (6), and the final NLRSC-MvSC model can be formulated as

$$\begin{aligned} &\min_{\mathbf{C}_v,\mathbf{E}_v} \sum_{v=1}^{V} \|\mathbf{C}_v\|_q^q + \lambda \sum_{v=1}^{V} \|\mathbf{W} \odot \mathbf{C}_v\|_q^q + \beta \sum_{v=1}^{V} \|\mathbf{E}_v\|_{2,q}, \\ &\quad \text{s.t. } \mathbf{X}_v = \mathbf{X}_v\mathbf{C}_v + \mathbf{E}_v, \forall v \in \{1, 2, \ldots, V\}, \end{aligned} \tag{7}$$

where λ is a trade-off parameter for balancing each term, $\odot$ denotes the Hadamard product [Zhang, 2017], and $\mathbf{W}_{i,j} \in [0, 1]$ represents the soft weight on each coefficient. Ideally, the coefficients of inter-cluster samples should be assigned the largest weight 1, while the smallest 0 is weighted on intra-cluster samples. However, the label information of data is unknown in unsupervised MvSC tasks. Aim to obtain an expected weight, a efficacious strategy is given as follows

$$\mathbf{W}_{i,j} = 1 - \exp\left(-\frac{1 - |\langle \mathbf{H}_{:,i}, \mathbf{H}_{:,j}\rangle|}{\xi}\right), \tag{8}$$

where $\langle \cdot, \cdot \rangle$ is the inner product, $\mathbf{H} = [\hat{\mathbf{X}}_1; \hat{\mathbf{X}}_2; \ldots; \hat{\mathbf{X}}_V]^T \in \mathbb{R}^{D\times n}$ with $D = d_1 + d_2 + \cdots + d_V$ denotes the vertical concatenation of all normalized feature sets $\hat{\mathbf{X}}_v$, and ξ is set to the average of all $1 - |\langle \mathbf{H}_{:,i}, \mathbf{H}_{:,j}\rangle|$s empirically. In this way, the angle information among confounding data points can be fully exploited for accurate subspace segmentation.

3.2 Optimization

By drawing on the powerful alternating direction method of multipliers (ADMM) [Kuybeda *et al.*, 2013; Liu *et al.*, 2023b] framework, the nonconvex and multi-variable problem arising by model (7) can be effectively solved with the following designed algorithm.

According to the ADMM method, we introduce two auxiliary variables into each view-specific subproblem for the separability of $\mathbf{C}_v$, and then (7) is equivalent to the following form.

$$\begin{aligned} &\min_{\mathbf{P}_v,\mathbf{S}_v,\mathbf{C}_v,\mathbf{E}_v} \|\mathbf{P}_v\|_q^q + \lambda\|\mathbf{W} \odot \mathbf{S}_v\|_q^q + \beta\|\mathbf{E}_v\|_{2,q} \\ &\quad \text{s.t. } \mathbf{X}_v = \mathbf{X}_v\mathbf{C}_v + \mathbf{E}_v, \mathbf{C}_v = \mathbf{P}_v, \mathbf{C}_v = \mathbf{S}_v. \end{aligned} \tag{9}$$

Now, the Augmented Lagrangian function of constrained problem (9) can be given with three dual multipliers $\mathbf{M}_{v,1}$,$\mathbf{M}_{v,2}$ and $\mathbf{M}_{v,3}$, i.e.,

$$\begin{aligned} &\mathcal{L}_\mu(\mathbf{P}_v, \mathbf{S}_v, \mathbf{C}_v, \mathbf{E}_v, \mathbf{M}_{v,1}, \mathbf{M}_{v,2}, \mathbf{M}_{v,3}) \\ &\quad = \|\mathbf{P}_v\|_q^q + \lambda\|\mathbf{W} \odot \mathbf{S}_v\|_q^q + \beta\|\mathbf{E}_v\|_{2,q} \\ &\quad + \Omega(\mathbf{M}_{v,1}, \mathbf{C}_v - \mathbf{P}_v) + \Omega(\mathbf{M}_{v,2}, \mathbf{C}_v - \mathbf{S}_v) \\ &\quad + \Omega(\mathbf{M}_{v,3}, \mathbf{X}_v - \mathbf{X}_v\mathbf{C}_v - \mathbf{E}_v), \end{aligned} \tag{10}$$

where $\Omega(\mathbf{A}, \mathbf{B}) = \langle \mathbf{A}, \mathbf{B}\rangle + (\mu/2)\|\mathbf{B}\|_F^2$, $\mu > 0$ is a penalty scalar. Then, the unconstrained problem (10) can be optimized by solving the subproblem of each variable alternately.

Update $\mathbf{P}_v$: Fixing the other variables, the subproblem involving with P_v can be written as

$$\begin{aligned}&\arg\min_{\mathbf{P}_v} \|\mathbf{P}_v\|_q^q + \Omega(\mathbf{M}_{v,1}, \mathbf{C}_v - \mathbf{P}_v)\\ &= \arg\min_{\mathbf{P}_v} \frac{1}{\mu}\|\mathbf{P}_v\|_q^q + \frac{1}{2}\|\mathbf{P}_v - (\mathbf{C}_v + \frac{\mathbf{M}_{v,1}}{\mu})\|_F^2. \quad (11)\end{aligned}$$

For simplicity, let $\mathbf{Y} = \mathbf{C}_v + \mathbf{M}_{v,1}/\mu$, and the SVD of $\mathbf{Y}$ be $\mathbf{U}\,\mathrm{Diag}(\sigma(\mathbf{Y}))\mathbf{V}^T$. Its solution can be achieved by the closed-form thresholding formulas in Lemma 1 and 2

$$\mathbf{P}_v^* = \mathbf{U}\,\mathrm{Diag}(\mathcal{H}_{\frac{1}{\mu},q}(\sigma(\mathbf{Y})))\mathbf{V}^T, \quad (12)$$

where $\mathcal{H}_{\lambda,q}(\mathbf{x}) = (h_{\lambda,q}(x_1), h_{\lambda,q}(x_2), \ldots, h_{\lambda,q}(x_n))$.

Update $\mathbf{S}_v$: Fixing the other variables, the subproblem involving with $\mathbf{S}_v$ can be written as

$$\begin{aligned}&\arg\min_{\mathbf{S}_v} \lambda\|\mathbf{W}\odot\mathbf{S}_v\|_q^q + \Omega(\mathbf{M}_{v,2}, \mathbf{C}_v - \mathbf{S}_v)\\ &= \arg\min_{\mathbf{S}_v} \frac{\lambda}{\mu}\|\mathbf{W}\odot\mathbf{S}_v\|_q^q + \frac{1}{2}\|\mathbf{S}_v - (\mathbf{C}_v + \frac{\mathbf{M}_{v,2}}{\mu})\|_F^2. \quad (13)\end{aligned}$$

Let $\mathbf{Y} = \mathbf{C}_v + \mathbf{M}_{v,2}/\mu$ and $\mathbf{B} = (\lambda/\mu)\mathbf{W}$. Similar to (11), we obtain

$$[\mathbf{S}_v^*]_{i,j} = h_{\mathbf{B}_{i,j},q}(\mathbf{Y}_{i,j}). \quad (14)$$

Update $\mathbf{C}_v$: Fixing the other variables, the subproblem involving with $\mathbf{C}_v$ can be written as

$$\begin{aligned}&\arg\min_{\mathbf{C}_v} \Omega(\mathbf{M}_{v,1}, \mathbf{C}_v - \mathbf{P}_v) + \Omega(\mathbf{M}_{v,2}, \mathbf{C}_v - \mathbf{S}_v)\\ &+ \Omega(\mathbf{M}_{v,3}, \mathbf{X}_v - \mathbf{X}_v\mathbf{C}_v - \mathbf{E}_v). \quad (15)\end{aligned}$$

The convex quadratic equation (15) can be easily solved by taking the derivative with respect to $\mathbf{C}_v$ and setting it to zero, we get

$$\mathbf{C}_v^* = (2\mu\mathbf{I} + \mu\mathbf{X}_v^T\mathbf{X}_v)^{-1}\widetilde{\mathbf{C}}_v, \quad (16)$$

where $\widetilde{\mathbf{C}}_v = \mathbf{X}_v^T(\mathbf{M}_{v,3} + \mu\mathbf{X}_v - \mu\mathbf{E}_v) + \mu\mathbf{P}_v + \mu\mathbf{S}_v - \mathbf{M}_{v,1} - \mathbf{M}_{v,2}$.

Update $\mathbf{E}_v$: Fixing the other variables, the variable $\mathbf{E}_v$ can be achieved by the following subproblem

$$\begin{aligned}&\arg\min_{\mathbf{E}_v} \beta\|\mathbf{E}_v\|_{2,q} + \Omega(\mathbf{M}_{v,3}, \mathbf{X}_v - \mathbf{X}_v\mathbf{C}_v - \mathbf{E}_v),\\ &= \arg\min_{\mathbf{E}_v} \frac{\beta}{\mu}\|\mathbf{E}_v\|_{2,q} + \frac{1}{2}\|\mathbf{E}_v - \widetilde{\mathbf{E}}_v\|_F^2, \quad (17)\end{aligned}$$

where $\widetilde{\mathbf{E}}_v = \mathbf{X}_v - \mathbf{X}_v\mathbf{C}_v + (1/\mu)\mathbf{M}_{v,3}$. Then, we have

$$[\mathbf{E}_v^*]_{i,j} = h_{\frac{\beta}{\mu},q}(\mathbf{Y}_{i,j}), \quad (18)$$

where $\mathbf{Y}$ can be obtained as [Liu *et al.*, 2012]

$$[\mathbf{Y}_v]_{:,j} = \frac{(\|[\widetilde{\mathbf{E}}_v]_{:,j}\|_2 - \frac{\beta}{\mu})_+}{\|[\widetilde{\mathbf{E}}_v]_{:,j}\|_2}[\widetilde{\mathbf{E}}_v]_{:,j}. \quad (19)$$

Algorithm 1 Algorithm for solving problem (9)

Input: Multi-view data $\{\mathbf{X}_1, \mathbf{X}_2 \ldots, \mathbf{X}_V\}$, weight matrix $\mathbf{W}$ and parameters λ, β, q.
Initialize: $\mathbf{C}_v = \mathbf{P}_v = \mathbf{S}_v = \mathbf{0}$, $\mathbf{E}_v = \mathbf{0}$, $\mathbf{M}_{v,1} = \mathbf{M}_{v,2} = \mathbf{M}_{v,3} = \mathbf{0}$, $\forall v \in \{1, 2, \ldots, V\}$; $\mu = 10^{-2}$, $\mu_{max} = 10^{10}$, $\rho = 2$; $\epsilon = 10^{-6}$.
Output: $\{\mathbf{C}_v^*\}_{v=1}^V$.

```
while not converged do
    for v = 1 : V do
        Update P_v by (12);
        Update S_v by (14);
        Update C_v by (16);
        Update E_v by (18);
        Update M_{v,1}, M_{v,2}, M_{v,3} and μ by (20)-(23);
    end for
    Check the convergence criterion: max{||C_v − P_v||_∞, ||C_v − S_v||_∞, ||X_v − X_v C_v − E_v||_∞} < ε
end while
```

Update $\mathbf{M}_{v,1}, \mathbf{M}_{v,2}, \mathbf{M}_{v,3}$ and μ: The multipliers and penalty scalar can be updated by

$$\begin{cases}\mathbf{M}_{v,1}^* = \mathbf{M}_{v,1} + \mu(\mathbf{C}_v - \mathbf{P}_v), & (20)\\ \mathbf{M}_{v,2}^* = \mathbf{M}_{v,2} + \mu(\mathbf{C}_v - \mathbf{S}_v), & (21)\\ \mathbf{M}_{v,3}^* = \mathbf{M}_{v,3} + \mu(\mathbf{X}_v - \mathbf{X}_v\mathbf{C}_v - \mathbf{E}_v), & (22)\\ \mu^* = \min(\rho\mu, \mu_{max}), & (23)\end{cases}$$

where $\rho > 1$ denotes the step size for convergence. The details of our proposed optimization scheme are stated in Algorithm 1.

With the obtained set of optimal subspace representations $\{\mathbf{C}_v^*\}_{v=1}^V$, the compact affinity graph $\mathbf{G}$ can be constructed by the following fusion mechanism

$$\mathbf{G} = \frac{1}{V}\sum_{v=1}^{V}|\mathbf{C}_v^*| + |\mathbf{C}_v^{*T}|. \quad (24)$$

Then, the clustering labels for MvSC can be achieved by conducting the spectral clustering [Ng *et al.*, 2001] on $\mathbf{G}$.

3.3 Theoretical Analysis

Computational Complexity. The time complexity of our proposed algorithm is mainly to solve the subproblems involving with $\mathbf{P}_v, \mathbf{S}_v, \mathbf{C}_v$ and $\mathbf{E}_v$, respectively. To be specific, updating $\mathbf{P}_v$ takes $\mathcal{O}(n^3)$ due to SVD operation. The complexity of updating $\mathbf{S}_v$ is $\mathcal{O}(n^2)$. For variable $\mathbf{C}_v$, its updating relies on the operations of SVD, matrix multiplication and inverse, thus the complexity is $\mathcal{O}(n^3 + n^2 d_v)$. Besides, updating $\mathbf{E}_v$ with matrix multiplication costs $\mathcal{O}(n^2 d_v)$ time. Consequently, the Algorithm 1 has the computational complexity of $\mathcal{O}(KVn^3)$ (assuming $d_{max} \leq n$), where $d_{max} = \max\{d_1, d_2, \ldots, d_V\}$, K denotes the number of iterations.

Convergence Analysis. In addition to the terrific performance, it is also indispensable to establish the rigorous convergence guarantee of the proposed algorithm. Thus, a reliable analysis is theoretically provided in following Theorem 1, which demonstrates that the sequence generated by

Dataset	Clu./Sam.	Dimension
Yale	15/165	4096/3304/6750
MSRC-v1	7/210	1302/512/256/210/100/48
BBC4view	5/685	4659/4633/4665/4684
100leaves	100/1600	64/64/64
ProteinFold	27/694	694/694/694/...[1]

[1] The dimensions of all 12 views are 694.

Table 1: Statistical details of benchmark datasets. Clu. and Sam. denote the Cluster and Sample, respectively.

our proposed algorithm converges to a stationary KKT critical point. The detailed proof is provided in the supplementary material [1].

Theorem 1. *Let the sequence* $\{\Theta^k = (\mathbf{C}_v^k,\ \mathbf{P}_v^k,\ \mathbf{S}_v^k,\ \mathbf{E}_v^k;\ \mathbf{M}_{v,1}^k,\ \mathbf{M}_{v,2}^k,\ \mathbf{M}_{v,3}^k)\}_{k=1}^{\infty}$ *be generated by Algorithm 1. Then, we have*

1) *The sequence* $\{\Theta^k\}_{k=1}^{\infty}$ *is bounded, and has at least one accumulation point.*
2) *Any accumulation point* Θ^* *satisfies*

$$\begin{cases} \mathbf{C}_v^* - \mathbf{P}_v^* = \mathbf{0}, & (25)\\ \mathbf{C}_v^* - \mathbf{S}_v^* = \mathbf{0}, & (26)\\ \mathbf{X}_v - \mathbf{X}_v\mathbf{C}_v^* - \mathbf{E}_v^* = \mathbf{0}, & (27)\\ \mathbf{M}_{v,1}^* \in \partial_{\mathbf{P}_v}\|\mathbf{P}_v^*\|_q^q, & (28)\\ \mathbf{M}_{v,2}^* \in \lambda\partial_{\mathbf{S}_v}\|\mathbf{W}\odot\mathbf{S}_v^*\|_q^q, & (29)\\ \mathbf{M}_{v,3}^* \in \beta\partial_{\mathbf{E}_v}\|\mathbf{E}_v^*\|_{2,q}. & (30) \end{cases}$$

4 Experiments

In this section, we evaluate our proposed NLRSC-MvSC model on five benchmark datasets in comparison with ten representative clustering models. Then, the clustering performance and robustness of NLRSC-MvSC are analyzed.

4.1 Datasets and Experimental Setting

Datasets. In our experiments, five popular datasets under different clustering scenarios are selected. Their brief descriptions are reported as follows, and detailed statistical data are shown in Table 1.

- **Yale** is a face dataset which contains 165 data samples from 15 subjects in each view. And three types of features are extracted, i.e., Intensity, LBP and Gabor.
- **MSRC-v1** is a object dataset. It consists of 7 subjects with 210 images in each view. Six image features are adopted, that is, HOG, SIFT, LBP, CENT, GIST and CMT.
- **BBC4view** is a news text dataset with four different views. Each includes 685 documents from five topics.
- **100leaves** is a object dataset consists of 1600 leaf samples belonging to 100 plant species. The shape, margin and texture features of each leaf are employed as three different views.
- **ProteinFold** contains 12 distinct view features. Each has 27-fold classes with 694 protein domains.

[1]https://github.com/wangzhi-swu/NLRSC-MvSC.

Method	ACC ↑	NMI ↑	ARI ↑	F1 ↑
LRR_{Concat}	0.6848	0.7185	0.5092	0.5416
DiMvSC	0.6485	0.6914	0.5034	0.5344
LMvSC	0.7030	0.7191	0.5164	0.5476
MvLRSSC-P	0.6424	0.6741	0.4860	0.5183
MvLRSSC-C	0.7091	0.7280	0.5546	0.5823
LS-MvSC	0.6424	0.6717	0.4737	0.5077
MvLRR	0.6970	0.7148	0.5263	0.5563
EOMvSC-CA	0.6242	0.6317	0.4207	0.4592
MvLPL	0.6909	0.7021	0.4951	0.5292
MMvGC	0.6848	0.6917	0.4811	0.5140
Ours($q = 2/3$)	**0.7455**	**0.7769**	**0.6213**	**0.6452**
Ours($q = 1/2$)	<u>0.7394</u>	<u>0.7696</u>	<u>0.6092</u>	<u>0.6339</u>

Table 2: Clustering results on **Yale** dataset.

Method	ACC ↑	NMI ↑	ARI ↑	F1 ↑
LRR_{Concat}	0.8095	0.7010	0.6343	0.6860
DiMvSC	0.6619	0.5385	0.4305	0.5114
LMvSC	0.8571	0.7446	0.7072	0.7482
MvLRSSC-P	0.7952	0.6719	0.6157	0.6697
MvLRSSC-C	0.7905	0.6743	0.6119	0.6665
LS-MvSC	0.8333	0.7435	0.6722	0.7188
MvLRR	0.8524	0.7341	0.6908	0.7343
EOMvSC-CA	0.8476	0.7555	0.7141	0.7556
MvLPL	0.7905	0.7028	0.5669	0.6310
MMvGC	0.8857	0.7917	0.7550	0.7891
Ours($q = 2/3$)	<u>0.8952</u>	**0.8131**	<u>0.7708</u>	<u>0.8030</u>
Ours($q = 1/2$)	**0.9000**	<u>0.8092</u>	**0.7799**	**0.8107**

Table 3: Clustering results on **MSRC-v1** dataset.

Compared Models. In order to demonstrate the superiority of our proposed model, ten representative clustering models are selected as the competitors. One of them is the classical LRR model, which performs single-view clustering on the features that concatenated by all views. The rest are multi-view clustering models, including DiMvSC [Cao *et al.*, 2015], LMvSC [Zhang *et al.*, 2017], MvLRSSC-Pairwise [Brbić and Kopriva, 2018], MvLRSSC-Centroid [Brbić and Kopriva, 2018], LS-MvSC [Kang *et al.*, 2020], MvLRR [Chen *et al.*, 2022], EOMvSC-CA [Liu *et al.*, 2022], MvLPL [Liu *et al.*, 2023a] and MMvGC [Tan *et al.*, 2023]. To ensure fairness, we run the source codes provided by their authors with the parameters recommended in articles.

Clustering Metrics. Four metrics are employed as the comprehensive evaluation of clustering performance, including accuracy (**ACC**), normalized mutual information (**NMI**), adjusted rand index (**ARI**) and F1-score (**F1**). The higher the scores of metrics, the better the clustering performance. All experiments are conducted by MATLAB R2020b on a Workstation with Intel(R) Xeon(R) Gold 6230 CPU@2.10GHz and 256GB RAM.

Method	ACC ↑	NMI ↑	ARI ↑	F1 ↑
LRR_{Concat}	0.8526	0.6819	0.7006	0.7687
DiMvSC	0.9182	0.7682	0.8197	0.8616
LMvSC	0.8628	0.6582	0.7001	0.7707
MvLRSSC-P	0.8569	0.6928	0.7277	0.7909
MvLRSSC-C	0.8599	0.7007	0.7364	0.7978
LS-MvSC	0.7708	0.6061	0.5220	0.6344
MvLRR	0.8555	0.6961	0.7021	0.7698
EOMvSC-CA	0.4204	0.0717	0.0942	0.3547
MvLPL	0.8248	0.6140	0.6331	0.7242
MMvGC	0.9212	0.7697	0.8165	0.8591
Ours($q = 2/3$)	<u>0.9255</u>	<u>0.7964</u>	<u>0.8348</u>	<u>0.8741</u>
Ours($q = 1/2$)	**0.9270**	**0.7980**	**0.8373**	**0.8758**

Table 4: Clustering results on **BBC4view** dataset.

Method	ACC ↑	NMI ↑	ARI ↑	F1 ↑
LRR_{Concat}	0.7769	0.8938	0.7004	0.7033
DiMvSC	0.5756	0.7594	0.4125	0.4182
LMvSC	0.7450	0.8696	0.6471	0.6506
MvLRSSC-P	0.7750	0.8960	0.6992	0.7022
MvLRSSC-C	0.7650	0.8944	0.6991	0.7021
LS-MvSC	0.7488	0.8845	0.6556	0.6592
MvLRR	0.7688	0.8944	0.6969	0.6999
EOMvSC-CA	0.4462	0.7015	0.2583	0.2696
MvLPL	0.6956	0.8321	0.5834	0.5872
MMvGC	0.7819	0.8887	0.7008	0.7037
Ours($q = 2/3$)	**0.8069**	<u>0.9049</u>	**0.7412**	**0.7437**
Ours($q = 1/2$)	<u>0.7981</u>	**0.9054**	<u>0.7322</u>	<u>0.7348</u>

Table 5: Clustering results on **100leaves** dataset.

4.2 Performance Evaluation

The clustering performance on five datasets of all competing methods are listed in Table 2 - Table 6. The highest and second highest scores are marked in **bold** and <u>underline</u>, respectively. Then, the experimental results are analyzed as follows

- It can be seen that our proposed methods can always achieve the highest scores on all metrics and datasets. For instance, on Yale dataset, NLRSC-MvSC ($q = 2/3$) significantly improves the scores in terms of ACC, NMI, ARI and F1 by 3.64%, 4.89%, 6.67% and 6.29% compared to others. This indicates that the proposed model can fully utilize the consistency and complementarity of multi-view features, thereby contributing to learn a more comprehensive subspace representation.
- In order to verify the performance improvement of the consistent structural constraint in NLRSC-MvSC, we visualize the affinity graphs produced by different methods in Figure 2. It can be observed intuitively that the affinity graph constructed by our method exhibits a more distinct block diagonal structure with less deceptive pairwise correlations, as marked in MvLRR and MMvGC graphs by red boxes. Thus, our graph can provide more discriminable subspace information for clustering process. In addition, the block saliency of obtained graphs can be quantitatively measured by the Contrast Index (CI), which is defined as [Li *et al.*, 2019b]

$$\text{CI} = \frac{\mathbf{D}_{sum}}{\mathbf{D}_{sum} + \mathbf{N}_{sum}} = \frac{\mathbf{D}_{sum}}{\|\mathbf{G}\|_1}, \tag{31}$$

where $\mathbf{D}_{sum}$ and $\mathbf{N}_{sum}$ denote the summation of affinity values belonging to the diagonal and nondiagonal blocks, respectively. As shown in Table 7, NLRSC-MvSC achieves the highest score in comparison with several state-of-the-art methods. This can be attributed to the accurate subspace segmentation of confounding samples under the structural constraint.
- Furthermore, we apply the t-distributed stochastic neighbor embedding (t-SNE) technique [van der Maaten and Hinton, 2008] to compare the low rankness of fusion representations learned by NLRSC-MvSC and other nuclear norm-based methods. Specifically, we first obtain

Method	ACC ↑	NMI ↑	ARI ↑	F1 ↑
LRR_{Concat}	**0.3818**	0.4490	0.1992	0.2352
DiMvSC	0.1542	0.2267	0.0246	0.0671
LMvSC	0.3401	0.4179	0.1716	0.2079
MvLRSSC-P	0.2824	0.3765	0.1399	0.1785
MvLRSSC-C	0.2867	0.3761	0.1364	0.1736
LS-MvSC	0.3415	0.4262	0.1504	0.1989
MvLRR	0.3084	0.3956	0.1485	0.1856
EOMvSC-CA	0.2608	0.3474	0.1244	0.1697
MvLPL	0.3588	0.4410	0.1617	0.2086
MMvGC	<u>0.3761</u>	0.4542	0.2094	0.2435
Ours($q = 2/3$)	**0.3818**	**0.4728**	**0.2231**	**0.2572**
Ours($q = 1/2$)	0.3631	<u>0.4724</u>	<u>0.2178</u>	<u>0.2517</u>

Table 6: Clustering results on **ProteinFold** dataset.

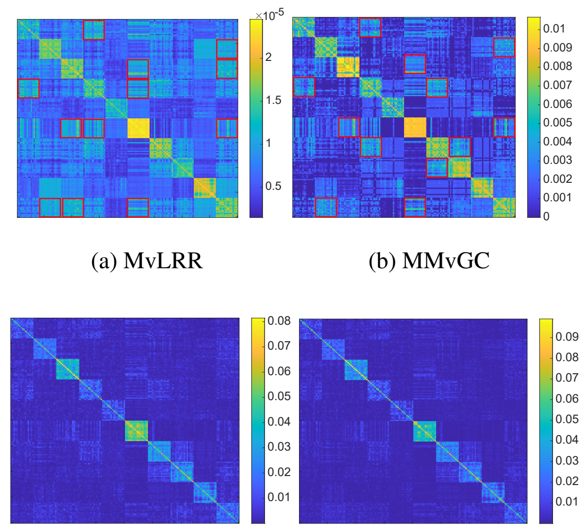

(a) MvLRR (b) MMvGC

(c) Ours ($q = 2/3$) (d) Ours ($q = 1/2$)

Figure 2: Affinity graphs constructed by different methods on 100leaves dataset (only first 10 subjects selected).

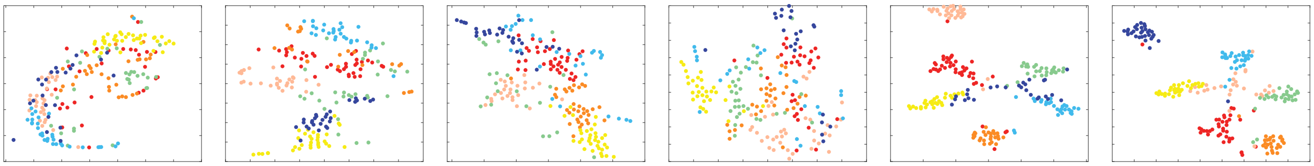

(a) LMvSC (b) MvLRSSC-P (c) MvLRSSC-C (d) MvLRR (e) Ours ($q = 2/3$) (f) Ours ($q = 1/2$)

Figure 3: The visualizations on MSRC-v1 dataset by t-SNE.

	DiMSC	LMSC	MLRSSC-P	MLRSSC-C
CI ↑	0.0806	0.2378	0.1252	0.1424
	MLRR	MMGC	Ours(2/3)	Ours(1/2)
CI ↑	0.1110	0.1853	0.2796	**0.3138**

Table 7: CI of the obtained affinity graphs.

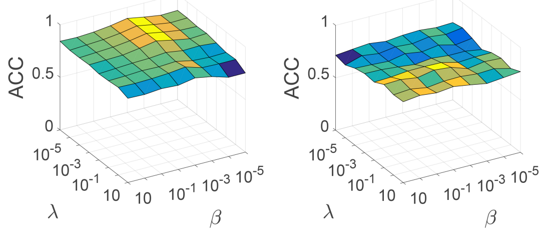

(a) MSRC-v1 ($q = 2/3$) (b) 100leaves ($q = 2/3$)

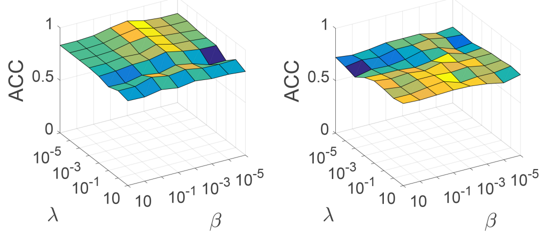

(c) MSRC-v1 ($q = 1/2$) (d) 100leaves ($q = 1/2$)

Figure 4: The parameters sensitivity on two datasets.

the cluster indicator matrix $\mathbf{F}$ by solving the following Laplacian embedding problem [Gao *et al.*, 2015]

$$\min_{\mathbf{F}} \operatorname{Tr}(\mathbf{F}^T \mathbf{L_G} \mathbf{F}) \quad \text{s.t. } \mathbf{F}^T\mathbf{F} = \mathbf{I}, \tag{32}$$

where $\mathbf{L_G} = \mathbf{A} - \mathbf{G}$ is Laplacian matrix, $\mathbf{G}$ can be constructed by (24), and $\mathbf{A}$ denotes a diagonal matrix with elements $\mathbf{A}_{i,i} = \sum_j \mathbf{G}_{i,j}$. The optimal $\mathbf{F} \in \mathbb{R}^{n\times c}$ can be yield by the eigenvectors of $\mathbf{L_G}$ corresponding to the smallest c eigenvalues, where c is the number of clusters. Then, a 2-D visualization of the clustering quality can be plotted by t-SNE with input $\mathbf{F}$. It can be seen in Figures 3e and 3f that there exist more larger gaps between the clusters dyed in different colours, while the points in same cluster are closer to each other. This means that

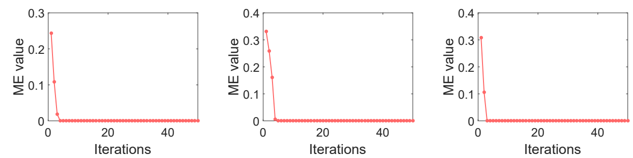

(a) MSRC-v1 (b) BBC4view (c) ProteinFold

Figure 5: The convergence curves on three datasets.

the coefficient matrix learned by NLRSC-MvSC has a more compact and lower-rank subspace structure, which better reflects the superiority of nonconvex ℓ_q regularization in terms of complementarity preserving.

4.3 Discussions

Parameter Sensitivity. Here, we tune the model parameters λ and β in a wide range, i.e., $\{10^{-6}, 10^{-5}, \ldots, 1, 10\}$ and show their impact on the clustering performance of two datasets in Figure 4. It can be seen that the ACC metric of NLRSC-MvSC stably remains at a relatively higher score, which implies that our method has the robust capability to cope with various clustering perturbations. Generally, the better clustering results can be obtained with the moderate λ and β, such as $\{10^{-3}, 10^{-2}, 10^{-1}\}$.

Numerical Convergence. In spite of the rigorous convergence analysis of the proposed algorithm given in Theorem 1, we also experimentally record the Maximum Error (ME) value during iterations, which is defined as $\mathrm{ME} = \max\{\mathrm{Err}_1, \mathrm{Err}_2, \ldots, \mathrm{Err}_V\}$, where $\mathrm{Err}_v = \max\{\|\mathbf{C}_v - \mathbf{P}_v\|_\infty, \|\mathbf{C}_v - \mathbf{S}_v\|_\infty, \|\mathbf{X}_v - \mathbf{X}_v\mathbf{C}_v - \mathbf{E}_v\|_\infty\}$. As presented in Figure 5, the curves on three datasets rapidly drop to 0 within about 5 iterations and remain smooth thereafter, which demonstrates that our algorithm can achieve convergence efficiently and reliably.

5 Conclusion

In this paper, we proposed a novel NLRSC-MvSC model by employing the nonconvex ℓ_q regularization for multi-view data clustering. Thanks to the proposed model, the intrinsic global low-rank structure in multi-view data can be efficiently captured, and confounding points can be carefully handled. As a result, a more comprehensive subspace representation can be learned. Extensive experiment results on various datasets show the superiority of our proposed model in clustering performance.

Acknowledgments

This work was supported in part by the Natural Science Foundation of China under Grant 72374173, in part by the Fundamental Research Funds for the Central Universities under Grant SWU-XDJH202303, and in part by Chongqing Innovative Research Groups under Grant CXQT21005.

References

[Basri and Jacobs, 2003] Ronen Basri and David W Jacobs. Lambertian reflectance and linear subspaces. *IEEE Transactions on Pattern Analysis and Machine Intelligence*, 2003.

[Brbić and Kopriva, 2018] Maria Brbić and Ivica Kopriva. Multi-view low-rank sparse subspace clustering. *Pattern Recognition*, 2018.

[Cai *et al.*, 2011] Deng Cai, Xiaofei He, Jiawei Han, and Thomas S Huang. Graph regularized nonnegative matrix factorization for data representation. *IEEE Transactions on Pattern Analysis and Machine Intelligence*, 2011.

[Cao *et al.*, 2013] Wenfei Cao, Jian Sun, and Zongben Xu. Fast image deconvolution using closed-form thresholding formulas of l_q $(q = 1/2, 2/3)$ regularization. *Journal of Visual Communication and Image Representation*, 2013.

[Cao *et al.*, 2015] Xiaochun Cao, Changqing Zhang, Huazhu Fu, Si Liu, and Hua Zhang. Diversity-induced multi-view subspace clustering. In *CVPR*, 2015.

[Chartrand and Yin, 2008] Rick Chartrand and Wotao Yin. Iteratively reweighted algorithms for compressive sensing. In *ICASSP*, 2008.

[Chartrand, 2007] Rick Chartrand. Exact reconstruction of sparse signals via nonconvex minimization. *IEEE Signal Processing Letters*, 2007.

[Chen *et al.*, 2022] Jie Chen, Shengxiang Yang, Hua Mao, and Conor Fahy. Multiview subspace clustering using low-rank representation. *IEEE Transactions on Cybernetics*, 2022.

[Elhamifar and Vidal, 2013] Ehsan Elhamifar and René Vidal. Sparse subspace clustering: Algorithm, theory, and applications. *IEEE Transactions on Pattern Analysis and Machine Intelligence*, 2013.

[Fang *et al.*, 2023] Uno Fang, Man Li, Jianxin Li, Longxiang Gao, Tao Jia, and Yanchun Zhang. A comprehensive survey on multi-view clustering. *IEEE Transactions on Knowledge and Data Engineering*, 2023.

[Gao *et al.*, 2015] Hongchang Gao, Feiping Nie, Xuelong Li, and Heng Huang. Multi-view subspace clustering. In *ICCV*, 2015.

[Ho *et al.*, 2003] Jeffrey Ho, Ming-Husang Yang, Jongwoo Lim, Kuang-Chih Lee, and David Kriegman. Clustering appearances of objects under varying illumination conditions. In *CVPR*, 2003.

[Kang *et al.*, 2020] Zhao Kang, Wangtao Zhou, Zhitong Zhao, Junming Shao, Meng Han, and Zenglin Xu. Large-scale multi-view subspace clustering in linear time. In *AAAI*, 2020.

[Kuybeda *et al.*, 2013] Oleg Kuybeda, Gabriel A Frank, Alberto Bartesaghi, Mario Borgnia, Sriram Subramaniam, and Guillermo Sapiro. A collaborative framework for 3d alignment and classification of heterogeneous subvolumes in cryo-electron tomography. *Journal of Structural Biology*, 2013.

[Li *et al.*, 2019a] Ruihuang Li, Changqing Zhang, Qinghua Hu, Pengfei Zhu, and Zheng Wang. Flexible multi-view representation learning for subspace clustering. In *IJCAI*, 2019.

[Li *et al.*, 2019b] Xuelong Li, Quanmao Lu, Yongsheng Dong, and Dacheng Tao. Robust subspace clustering by cauchy loss function. *IEEE Transactions on Neural Networks and Learning Systems*, 2019.

[Liu *et al.*, 2010] Guangcan Liu, Zhouchen Lin, and Yong Yu. Robust subspace segmentation by low-rank representation. In *ICML*, 2010.

[Liu *et al.*, 2012] Guangcan Liu, Zhouchen Lin, Shuicheng Yan, Ju Sun, Yong Yu, and Yi Ma. Robust recovery of subspace structures by low-rank representation. *IEEE Transactions on Pattern Analysis and Machine Intelligence*, 2012.

[Liu *et al.*, 2022] Suyuan Liu, Siwei Wang, Pei Zhang, Kai Xu, Xinwang Liu, Changwang Zhang, and Feng Gao. Efficient one-pass multi-view subspace clustering with consensus anchors. In *AAAI*, 2022.

[Liu *et al.*, 2023a] Baoyu Liu, Ling Huang, Changdong Wang, Jianhuang Lai, and Philip S Yu. Multiview clustering via proximity learning in latent representation space. *IEEE Transactions on Neural Networks and Learning Systems*, 2023.

[Liu *et al.*, 2023b] Tianyu Liu, Dong Hu, Zhi Wang, Jianping Gou, and Wu Chen. Hyperspectral image denoising using nonconvex fraction function. *IEEE Geoscience and Remote Sensing Letters*, 2023.

[Liu *et al.*, 2023c] Zhuo Liu, Dong Hu, Zhi Wang, Jianping Gou, and Tao Jia. Latlrr for subspace clustering via reweighted frobenius norm minimization. *Expert Systems with Applications*, 2023.

[Luo *et al.*, 2018] Shirui Luo, Changqing Zhang, Wei Zhang, and Xiaochun Cao. Consistent and specific multi-view subspace clustering. In *AAAI*, 2018.

[Ma *et al.*, 2008] Yi Ma, Allen Y Yang, Harm Derksen, and Robert Fossum. Estimation of subspace arrangements with applications in modeling and segmenting mixed data. *SIAM Review*, 2008.

[Marjanovic and Solo, 2012] Goran Marjanovic and Victor Solo. On l_q optimization and matrix completion. *IEEE Transactions on Signal Processing*, 2012.

[Muja and Lowe, 2014] Marius Muja and David G Lowe. Scalable nearest neighbor algorithms for high dimensional data. *IEEE Transactions on Pattern Analysis and Machine Intelligence*, 2014.

[Ng *et al.*, 2001] Andrew Ng, Michael Jordan, and Yair Weiss. On spectral clustering: Analysis and an algorithm. In *NeurIPS*, 2001.

[Qu *et al.*, 2022] Qin Qu, Zhi Wang, and Wu Chen. Robust subspace clustering based on latent low-rank representation with weighted schatten-p norm minimization. In *PRICAI*, 2022.

[Shan *et al.*, 2023] Yiwen Shan, Dong Hu, Zhi Wang, and Tao Jia. Multi-channel nuclear norm minus frobenius norm minimization for color image denoising. *Signal Processing*, 2023.

[Slepčev and Thorpe, 2019] Dejan Slepčev and Matthew Thorpe. Analysis of p-laplacian regularization in semisupervised learning. *SIAM Journal on Mathematical Analysis*, 2019.

[Tan *et al.*, 2023] Yuze Tan, Yixi Liu, Hongjie Wu, Jiancheng Lv, and Shudong Huang. Metric multi-view graph clustering. In *AAAI*, 2023.

[Tang *et al.*, 2014] Kewei Tang, Risheng Liu, Zhixun Su, and Jie Zhang. Structure-constrained low-rank representation. *IEEE Transactions on Neural Networks and Learning Systems*, 2014.

[Tang *et al.*, 2023] Kewei Tang, Kaiqiang Xu, Wei Jiang, Zhixun Su, Xiyan Sun, and Xiaonan Luo. Selecting the best part from multiple laplacian autoencoders for multi-view subspace clustering. *IEEE Transactions on Knowledge and Data Engineering*, 2023.

[van der Maaten and Hinton, 2008] Laurens van der Maaten and Geoffrey Hinton. Visualizing data using t-sne. *Journal of Machine Learning Research*, 2008.

[Vidal *et al.*, 2008] René Vidal, Roberto Tron, and Richard Hartley. Multiframe motion segmentation with missing data using powerfactorization and gpca. *International Journal of Computer Vision*, 2008.

[Vidal, 2011] René Vidal. Subspace clustering. *IEEE Signal Processing Magazine*, 2011.

[Wang *et al.*, 2019] Zhi Wang, Wendong Wang, Jianjun Wang, and Siqi Chen. Fast and efficient algorithm for matrix completion via closed-form $2/3$-thresholding operator. *Neurocomputing*, 2019.

[Wang *et al.*, 2020] Zhi Wang, Chao Gao, Xiaohu Luo, Ming Tang, Jianjun Wang, and Wu Chen. Accelerated inexact matrix completion algorithm via closed-form q-thresholding ($q = 1/2, 2/3$) operator. *International Journal of Machine Learning and Cybernetics*, 2020.

[Wang *et al.*, 2021] Zhi Wang, Dong Hu, Xiaohu Luo, Wendong Wang, Jianjun Wang, and Wu Chen. Performance guarantees of transformed schatten-1 regularization for exact low-rank matrix recovery. *International Journal of Machine Learning and Cybernetics*, 2021.

[Wang *et al.*, 2022] Zhi Wang, Yu Liu, Xin Luo, Jianjun Wang, Chao Gao, Dezhong Peng, and Wu Chen. Large-scale affine matrix rank minimization with a novel nonconvex regularizer. *IEEE Transactions on Neural Networks and Learning Systems*, 2022.

[Xu *et al.*, 2012] Zongben Xu, Xiangyu Chang, Fengmin Xu, and Hai Zhang. $l_{1/2}$ regularization: A thresholding representation theory and a fast solver. *IEEE Transactions on Neural Networks and Learning Systems*, 2012.

[Yang *et al.*, 2008] Allen Y Yang, John Wright, Yi Ma, and S. Shankar Sastry. Unsupervised segmentation of natural images via lossy data compression. *Computer Vision and Image Understanding*, 2008.

[Zhang *et al.*, 2017] Changqing Zhang, Qinghua Hu, Huazhu Fu, Pengfei Zhu, and Xiaochun Cao. Latent multi-view subspace clustering. In *CVPR*, 2017.

[Zhang, 2017] Xian-Da Zhang. *Matrix Analysis and Applications*. Cambridge University Press, 2017.